Research Article Vol. 35, No. 4 / April 2018 / Journal of the Optical Society of America B 797

Journal of the Optical Society of America B

OPTICAL PHYSICS

Analysis of the slow-light effect in silicon wire waveguides with metamaterials

Satoshi Yamasaki,[1,*] Tomohiro Amemiya,[1,2] Zhichen Gu,[1] Junichi Suzuki,[1] Nobuhiko Nishiyama,[1,2] and Shigehisa Arai[1,2]

[1]Department of Electrical and Electronic Engineering, Tokyo Institute of Technology, 2-12-1-S9-5 Ookayama, Meguro, Tokyo 152-8552, Japan
[2]Laboratory for Future Interdisciplinary Research of Science and Technology, Institute of Innovative Research, Tokyo Institute of Technology, Tokyo, Japan
*Corresponding author: yamasaki.s.ae@m.titech.ac.jp

Received 27 November 2017; revised 19 February 2018; accepted 19 February 2018; posted 20 February 2018 (Doc. ID 314410); published 15 March 2018

Slow-light devices have been attracting a great amount of attention owing to their potential applications in future optical networks and information-processing systems. In this paper we propose two types of silicon wire waveguides with metamaterials, which are potentially applicable to the deceleration of light speed, and we analyze the slow-light effect by using the homogenization-based mode analysis method. The derived dispersion relation indicates that a group index larger than 70 can be obtained with a propagation loss of ∼0.7 dB/μm near the resonant frequency of the metamaterial.

OCIS codes: (160.3918) Metamaterials; (230.7370) Waveguides; (130.3120) Integrated optics devices.

https://doi.org/10.1364/JOSAB.35.000797

1. INTRODUCTION

Metamaterials are artificially structured materials that can exhibit remarkable characteristics that are not found in natural materials. Optical metamaterials offer new opportunities for innovation in the field of electromagnetic parameter design, such as the tuning of electric permittivity ε and magnetic permeability μ. Natural materials have a constant relative permeability equal to 1 at optical frequencies, as their magnetization cannot follow the alternating magnetic field of the optical waves. Therefore, only permittivity can be controlled in the design of conventional photonic devices. However, metamaterials represent a major breakthrough as a solution to this limitation and allow us to control the permeability (different from unity) in the optical frequency region [1,2]. This metamaterial paradigm facilitates further development of photonic devices with novel optical functionalities, such as the invisibility cloak [3–7] and superresolution imaging [8,9]. Especially, many types of waveguide-type optical metamaterial devices have been reported in recent years [10], such as the "trapped rainbow" light storage [11,12], ultracompact optical modulators [13], coherent perfect absorber (CPA)-laser combination for lasing and antilasing [14], unidirectional mode converters [15], and waveguide-integrated mode-selective nanoantennas [16].

One promising application of such metamaterials is the slow-light device, which can decelerate the group velocity of the guided light waves. In this paper, we analyze the slow-light effect in silicon (Si) wire waveguides with metamaterials that can be easily integrated with other Si-based photonic devices. These can potentially be applied to many functions in Si-based photonic integrated circuits (PICs) [17,18], e.g., tunable delay for optical buffers in photonic routers, enhancement of the optical interaction and the nonlinear effect, miniaturization of optical modulators and detectors, nanoimaging, high-density magnetic data-storage recording, light harvesting, nanoscale quantum and nonlinear optics, and so on.

To date, there have been extensive efforts toward producing a slow-light effect. Leading examples are electromagnetically induced transparency (EIT) [19–22] and photonic crystals (PhCs) [23,24]. However, EIT devices are not suitable for integration with other Si photonic devices, because they use atomic states of materials under the low-temperature condition, and PhC devices require a relatively complicated structure compared to conventional waveguide-based Si photonic devices [25,26].

The waveguides proposed in this paper can overcome all the above problems. If necessary, the slow-light effect can be produced simply by placing metamaterials at an appropriate position on a Si wire waveguide. Furthermore, the desired group index can be obtained by changing the structure of the metamaterials independent of that of the Si wire waveguide. The following sections first present the structure and the principle of our device, and then explain the method of electromagnetic analysis. The operation of the device is established by numerical calculation based on the finite-difference method. Accordingly, a group index larger than 70 can be obtained with a propagation loss of ∼0.7 dB/μm near the resonant frequency of the metamaterial.

2. CONCEPT AND DEVICE STRUCTURE

Figure 1 shows the proposed metamaterial waveguide compared with the Si waveguide. The layer structures of the Si waveguide and metamaterial waveguide are shown in Figs. 1(a) and 1(b), respectively. The metamaterial waveguide is based on the Si wire waveguide, where the upper cladding layer is replaced by the metamaterial layer, which has strong wavelength dispersion compared to the SiO_2 cladding layer.

The conceptual dispersion curves of the Si waveguide and the metamaterial waveguide are shown in Figs. 1(c) and 1(d), respectively. The dispersion curve of the Si waveguide makes a gradual transition from the light line for the cladding to that for the core layer. On the other hand, the dispersion curve of the metamaterial waveguide will be discontinuous, affected by the resonance of the metamaterial layer, resulting in a relatively large permeability change. Around the discontinuity point, which is equal to the resonant point of the metamaterial, the slope of the dispersion curve would drastically decrease, indicating a reduced group velocity of the propagating light.

We first decide the basic structure of the metamaterial to control the permeability of optical waveguides. Most PICs are designed to operate with TE-polarized light, so the metamaterial has to interact with the magnetic field of the TE-polarized light travelling in the waveguide. A split-ring resonator (SRR) structure is suitable for this purpose. It consists of an array of minute metal SRRs arranged periodically with a pitch smaller than the wavelength of light. An individual SRR is an enclosed loop with one or more gaps and operates as an LC resonant circuit consisting of an inductor formed by the SRR and a capacitor formed by the gaps [27]. The SRR metamaterial consisting of a single-layer array is reasonably compatible with planar waveguides because it can be easily formed on the surface of the waveguide.

Figures 2(a) and 2(b) show the proposed slow-light Si waveguides with two types of nanoscale metal SRRs, which we call the planar structure and the three-dimensional structure, respectively. The difference between them is only the direction of the arranged SRRs. Comparing the two structures, the advantage of the planar structure is the ease of the fabrication process. The planar metamaterials can be easily formed by electron beam lithography (EBL) and the lift-off process above the conventional Si wire waveguide. However, in order to form the three-dimensional metamaterials, an additional patterning of the intermediate photomask layer is required. Despite the more complicated fabrication process, the three-dimensional one can provide a stronger wavelength dispersion, as the direction of the induced magnetic field is the same as that of light propagation.

In the waveguide combined with the SRRs on its top surface, the magnetic field of the TE-polarized light links with the SRRs. If the frequency of the light is approximately equal to the resonant frequency of the SRR, a circulating current is induced in the SRRs, and this produces a magnetic dipole moment in response to the light. The waveguide consequently shows a nonzero magnetic susceptibility at the light frequency. The group velocity of the optical pulse propagating through the waveguide can be significantly reduced thanks to the huge dispersion of the permittivity and permeability induced by the SRR.

3. ANALYSIS METHODS OF THE SI WIRE WAVEGUIDE WITH METAMATERIALS

The dispersion relation of a device can finally be revealed by using a two-dimensional mode analysis, which gives us the wavelength-dependent effective refractive index of the waveguide. However, the analysis of the electromagnetic field around the metal SRR and the mode analysis through the waveguide should be carried out simultaneously in order to obtain the device characteristics, which will require a significant amount of time in the calculation. The homogenization-based waveguide-mode analysis [28–30] can solve such a problem. The analysis procedure is described as follows.

To study the propagation properties of light, we divide the waveguide into multiple layers to calculate the spatial dependence of the optical field. We also replace the SRR and its neighborhood with a (hypothetical) uniform layer with

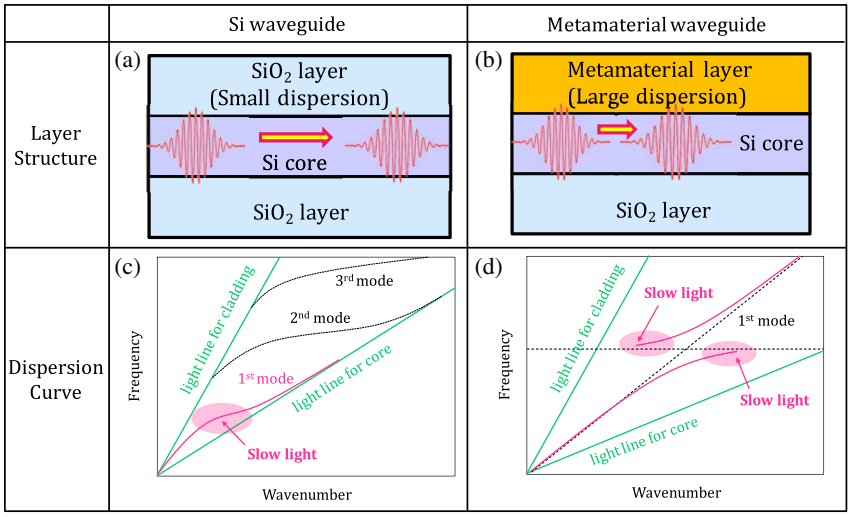

Fig. 1. Schematic images of the layer structures and the conceptual images of the dispersion curves of the metamaterial waveguide compared with those of the ordinary Si waveguide. Layer structures of (a) the Si waveguide and (b) the metamaterial waveguide. Dispersion curve of (c) the Si waveguide and (d) the metamaterial waveguide.

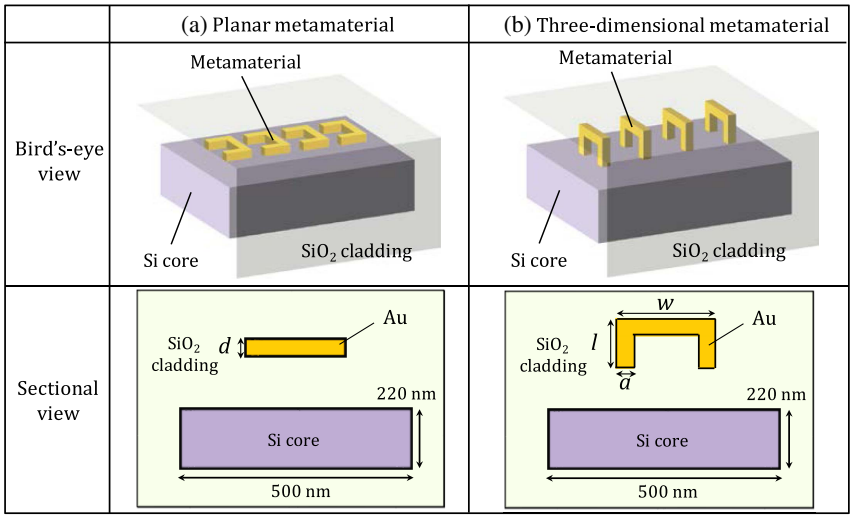

Fig. 2. Schematic images of two types of metamaterial waveguides with (a) planar metamaterial structure and (b) three-dimensional metamaterial structure.

appropriate values of permittivity and permeability. This metamaterial uniform layer has anisotropy derived from the operation of the SRR. Therefore, we should perform mode analysis with the permittivity and permeability tensors in an anisotropic material given by

$$\tilde{\varepsilon} = \begin{pmatrix} \varepsilon_x & 0 & 0 \\ 0 & \varepsilon_y & 0 \\ 0 & 0 & \varepsilon_z \end{pmatrix}, \qquad \tilde{\mu} = \begin{pmatrix} \mu_x & 0 & 0 \\ 0 & \mu_y & 0 \\ 0 & 0 & \mu_z \end{pmatrix}. \tag{1}$$

The effective values of permittivity ε_i and permeability μ_i $(i = x, y, z)$ of the metamaterial uniform layer can be determined as follows. Consider a unit cell of the metamaterial uniform layer for each SRR of the metamaterial [a dashed red box in Figs. 3(a) and 3(b)]. The unit cell is a cuboid whose length z and width x are equal to the array pitch of SRRs. Height y is set to an appropriate value of approximately one-quarter of the wavelength or less, as shown later. The equivalent values of ε and μ for the unit cell can be obtained from the scattering parameters (i.e., S_{11} and S_{21}) around the SRR calculated for incident electromagnetic waves introduced along the x, y, and z directions [see Fig. 3(c)] and given by [31–33]

$$\sqrt{\varepsilon_i}\sqrt{\mu_j} = \frac{1}{kd}\,\mathrm{Arccos}\left[\frac{1}{2S_{21}}(1 - S_{11}^2 + S_{21}^2)\right], \tag{2}$$

$$\frac{\sqrt{\mu_j}}{\sqrt{\varepsilon_i}} = \frac{\sqrt{(1 + S_{11})^2 - S_{21}^2}}{\sqrt{(1 - S_{11})^2 - S_{21}^2}}, \tag{3}$$

where k is the wavenumber of light. For example, ε_x and μ_z can be calculated from the set of S_{11} and S_{21}, shown in red in Fig. 3(c). Thus, the permeability and permittivity tensors of the metamaterial uniform layer can be obtained by considering anisotropy.

To analyze the characteristics considering the anisotropy of the metamaterial, the three parameters ε_x, μ_y, and μ_z, included in the following wave equation for the anisotropy waveguide, have to be derived:

$$\frac{\partial^2 E_x}{\partial y^2} + \left(\omega^2 \varepsilon_0 \mu_0 \varepsilon_x \mu_z - \beta^2 \frac{\mu_z}{\mu_y}\right) E_x = 0, \tag{4}$$

$$H_z = \frac{1}{j\omega\mu_0\mu_z}\frac{\partial E_x}{\partial y}, \tag{5}$$

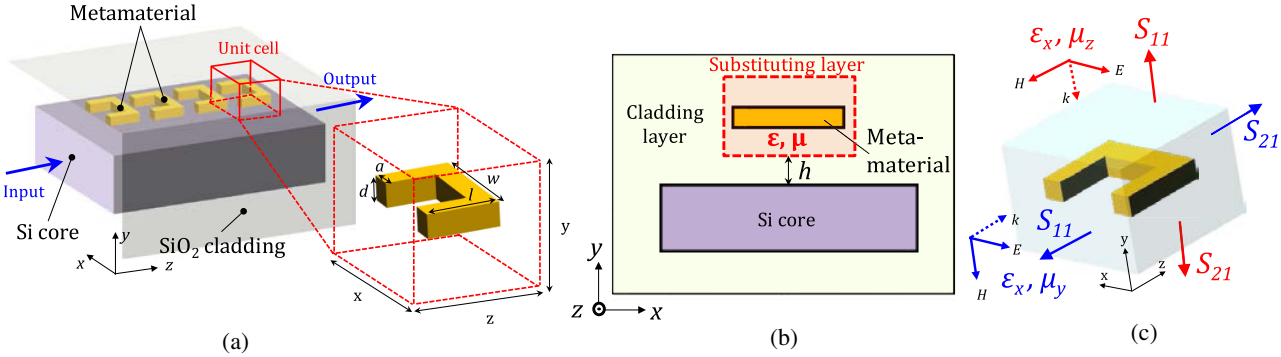

Fig. 3. (a) Si wire waveguide with an SRR line on its surface; (b) one example of the cross section of the waveguide; (c) retrieval of permittivity and permeability values from the S-parameter.

where β is the propagation constant in the device along the z direction, ω is the angular frequency, ε_0 is the permittivity of vacuum, μ_0 is the permeability of vacuum, and E_i and H_i ($i = x, y, z$) are the electric field (parallel to i axis) and magnetic field (parallel to i axis) of the light, respectively. We find from Eqs. (4) and (5) that E_x and H_z at the top of the device can be connected to E_x and H_z at the bottom of the device with the following transfer matrix:

$$\prod_m \begin{pmatrix} \cosh(\beta_m d_m) & \frac{j\omega\mu_0\mu_{zm}}{\beta_m}\sinh(\beta_m d_m) \\ \frac{\beta_m}{j\omega\mu_0\mu_{zm}}\sinh(\beta_m d_m) & \cosh(\beta_m d_m) \end{pmatrix}, \quad (6)$$

$$\beta_m = \sqrt{\beta^2\left(\frac{\mu_{zm}}{\mu_{ym}}\right) - k_0^2\varepsilon_{xm}\mu_{zm}}, \quad (7)$$

where ε_{xm} is the x component of the relative permittivity tensor, μ_{ym} and μ_{zm} are the y and z components of the permeability tensors in the mth layer, respectively, and d_m is the thickness of the mth layer.

At optical frequencies, the permeability tensors can be expressed using the identity matrix, except in the metamaterial uniform layer. Assuming an exponential decrease in E_x and H_z, outside a waveguide, we can solve Eq. (5) and obtain the effective refractive index($= \beta/k_0$). Combining this method with the conventional equivalent-index method [34] enables us to analyze the operation of the metamaterial waveguides.

4. ANALYSIS RESULTS AND DISCUSSION

A. Analysis of the Homogenization Layer for the Metamaterial

The transmission characteristics of the device, which are shown in Fig. 3(a), were estimated using COMSOL Multiphysics based on the finite-element method (FEM) [35].

First, we calculated the electromagnetic field over a cubic unit cell consisting of an individual nanoscale gold SRR. Considering mutual interactions of each SRR, we assumed perfect electric conductor (PEC) and perfect magnetic conductor (PMC) boundary conditions between unit cells to stimulate planar wave propagation in the y and z directions, as shown in Fig. 3(c) (an electric field was parallel to the SRR gap). In the simulation, the conductivity of the metal was defined by using the Drude model [36].

From the theoretical predictions of transmission spectra, we extracted the approximate constitutive parameter by using Eqs. (2) and (3). Figures 4(a) and 4(b) show the LC resonant frequencies of devices with planar and three-dimensional structures, respectively, as a function of SRR dimensions l and w [see Figs. 2 and 3(a)]; here, the SRR width a and thickness d were fixed to be 30 and 50 nm, respectively. The red lines show the contour line at 193 THz ($\lambda \approx 1.55$ μm). At LC resonant frequencies, the electric field can couple with the capacitance of the SRR and induce a circulating current, leading to a pronounced large-wavelength dispersion of permeability. With an increase in the SRR size, the resonant frequency decreased because of the enhancement of the loop inductance of the SRR. The dimensions of the individual SRR were determined as $l = 100$ nm, $w = 150$ nm, and $l = 110$ nm, $w = 140$ nm for the planar and three-dimensional structures, respectively, based on the simulation results shown in Fig. 4.

Figures 5(a) and 5(b) show the real and imaginary parts of the retrieved effective permittivity and permeability of the metamaterial uniform layer for the planar SRR ($l = 100$ nm, $w = 150$ nm) and three-dimensional SRR ($l = 110$ nm, $w = 140$ nm), respectively, calculated from 100 to 250 THz for the polarization direction of the incident light corresponding to those of Fig. 3(c). The permeability exhibits a strong and sharp resonance at ~190 THz, and we can see that all the parameters are drastically changing near the LC resonant frequency of the SRR.

B. Dispersion Curve Analysis

The dispersion relation can finally be revealed by using a two-dimensional mode analysis shown in Section 3, which gives us the effective refractive index of the waveguide with an assumed uniform distribution of the calculated permittivity and permeability inside the homogenized region of the Si waveguide.

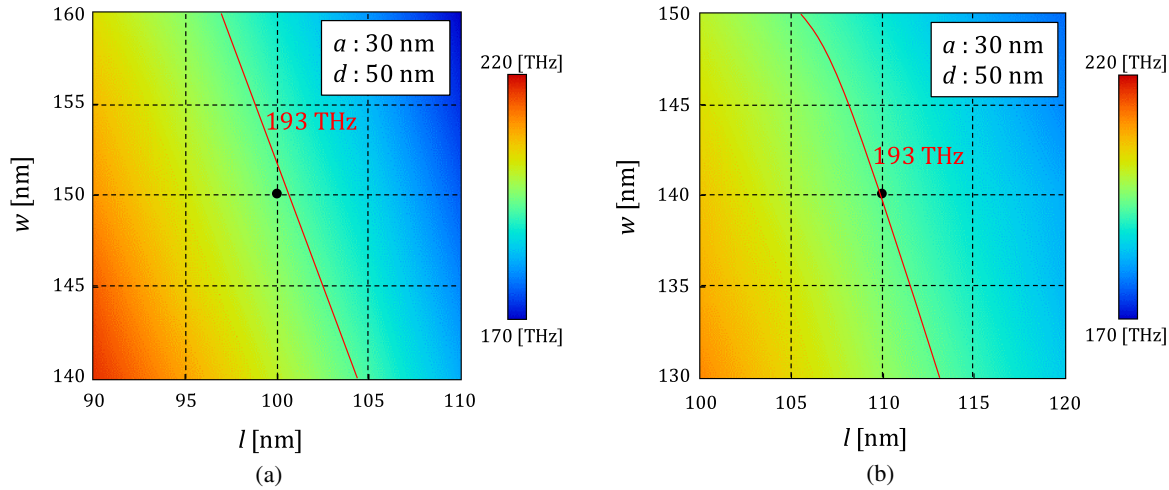

Fig. 4. Calculated resonance frequency as a function of the dimensions of the (a) planar metamaterial structure and (b) three-dimensional metamaterial structure.

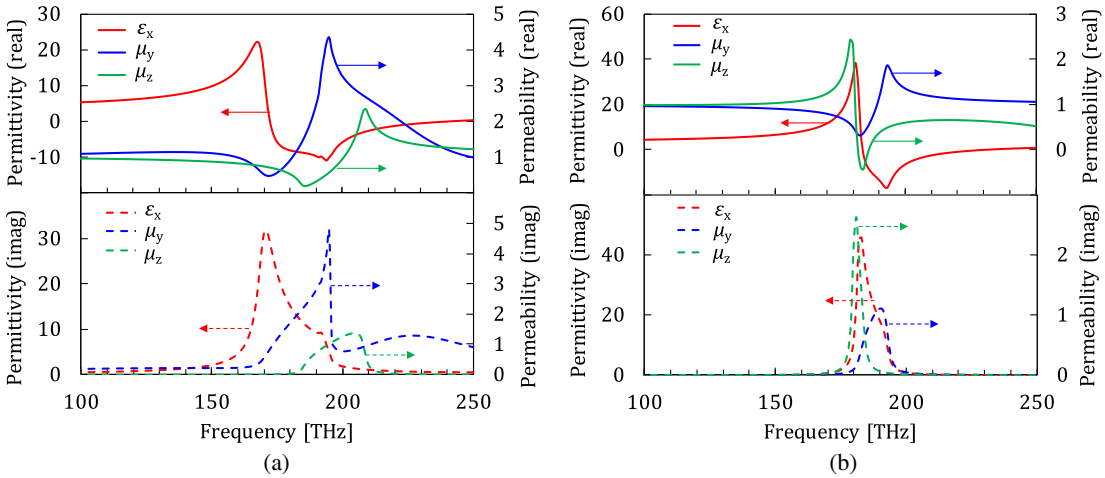

Fig. 5. Retrieved real and imaginary parts of relative permittivity ε_x and permeabilities μ_y and μ_z as a function of frequency, calculated for (a) a planar metamaterial structure ($l = 100$ nm, $w = 150$ nm) and (b) a three-dimensional metamaterial structure ($l = 110$ nm, $w = 140$ nm).

Figures 6(a) and 7(a) show the light lines of the SiO_2 cladding and the Si core (dashed black lines) and one example of the dispersion relation (red dots) with planar and three-dimensional metamaterial structures, respectively. During the calculation, we chose few points within the frequency range for simplifying the calculation and used the corresponding permittivity and permeability for each point, which is provided in Fig. 5. The slope of the dispersion curve drastically changes near the resonant frequency, and thereby causes the large variation in the permittivity and permeability. The blue dots in Figs. 6(a) and 7(a) also show the relationship between the dispersion and the imaginary part of the propagation constant (i.e., extinction coefficient), which indicates that the propagation loss increases when approaching the resonant frequency. The maximum extinction coefficient of ~0.2 corresponds to a propagation loss of ~0.7 dB/μm.

From these results, the group index n_g can be derived from the following equation:

$$n_g = c\frac{d\beta}{d\omega}, \tag{8}$$

where β and ω are the propagation constant and the angular frequency, respectively. Figures 6(b) and 7(b) show the group index n_g derived by the dispersion relation as a function of the wavelength. Reasonable n_g values greater than 40 and 70 were obtained near the discontinuity point for the devices with the planar and the three-dimensional metamaterial structures, respectively. Since the group index could not be defined accurately at the discontinuity point of the dispersion curve (i.e., the point where the group velocity is very close to zero), the energy velocity [37,38] should be considered rather than the group velocity at that point.

The delay can be significantly enhanced by increasing the number of rings, while the trade-off between the delay time and the propagation loss should be considered an important factor. In the device, light traveling along the Si waveguide

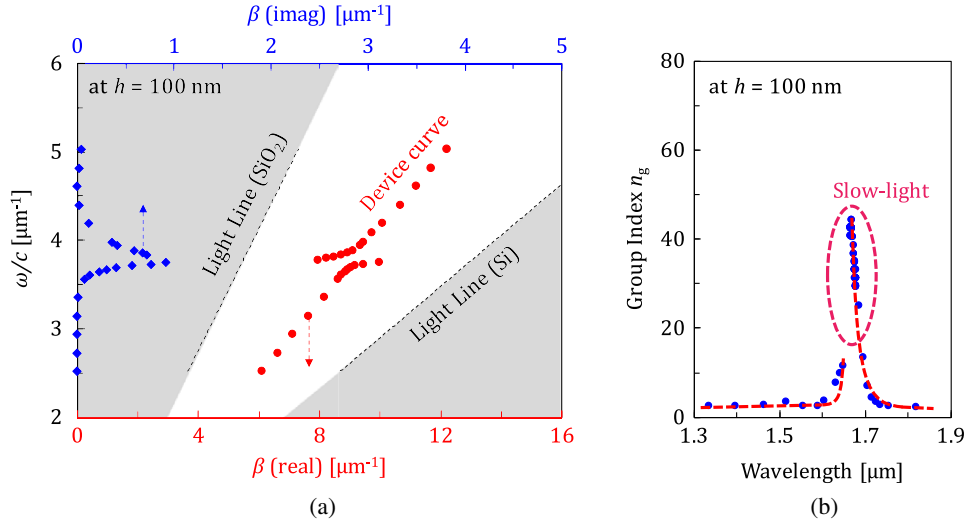

Fig. 6. (a) One example of the dispersion curve of the planar metamaterial structure [$h = 100$ nm in Fig. 3(b)]. (b) Group index n_g of the planar metamaterial structure as a function of wavelength.

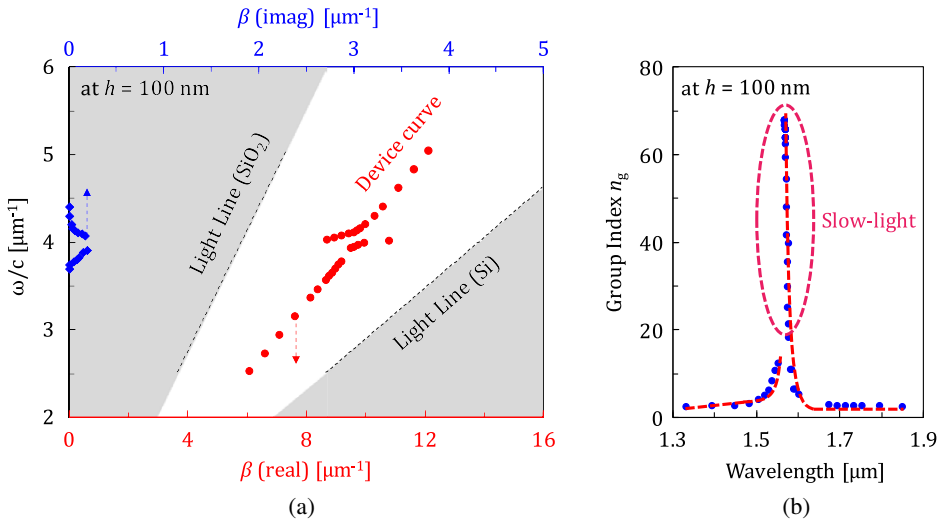

Fig. 7. (a) One example of the dispersion curve of the three-dimensional metamaterial structure [$h = 100$ nm in Fig. 3(b)]. (b) Group index n_g of the three-dimensional metamaterial structure as a function of wavelength.

propagates through the SiO_2 cladding layer into the metamaterial homogenization layer to a certain penetration depth and interacts with the metamaterials to ensure wavelength dispersion. Thus, the thickness of the SiO_2 cladding layer greatly affects the group index n_g. In particular, a large insertion loss is produced at a small cladding-layer thickness because a thin cladding layer easily allows light through to the metamaterial homogenization layer due to light absorption. Therefore, it is necessary to control the cladding layer thickness h [see Fig. 3(b)] to minimize the absorption loss under the condition that appropriate wavelength dispersion can be obtained.

To determine the optimum thickness of the SiO_2 cladding layer, we calculated the group index n_g and propagation loss of the device as a function of the thickness. Figure 8 summarizes the results, i.e., the group index n_g for the device with (a) planar and (b) three-dimensional metamaterial structures, together with the propagation loss as a function of the SiO_2 cladding layer thickness h. The device's absorption loss becomes larger at a smaller cladding thickness h because a part of the propagating light in the device leaks out of the cladding layer and is needlessly absorbed by the gold-based SRR. On the other hand, the group index rises to a certain level with an increase in h. For both structures, the highest group index could be obtained when $h = 100$ nm, and it would decrease over $h = 150$ nm. Under this condition, the highest group index of approximately 70 was achieved near the resonant frequency (~193 THz) with a propagation loss of 0.7 dB/μm for the device with the three-dimensional metamaterial structure, which can achieve ~1 ps delay time when 3-dB signal loss is allowable. The obtained value of the propagation loss is larger than the previously reported works such as the PhC devices [39], while we can expect a higher attainable group index within a wider frequency range thanks to the resonant point. A better delay time can be expected with a greater waveguide length with the compensation of optical loss by gain [40]. Taking the easiness to integrate on the Si platform into consideration, the hybrid semiconductor

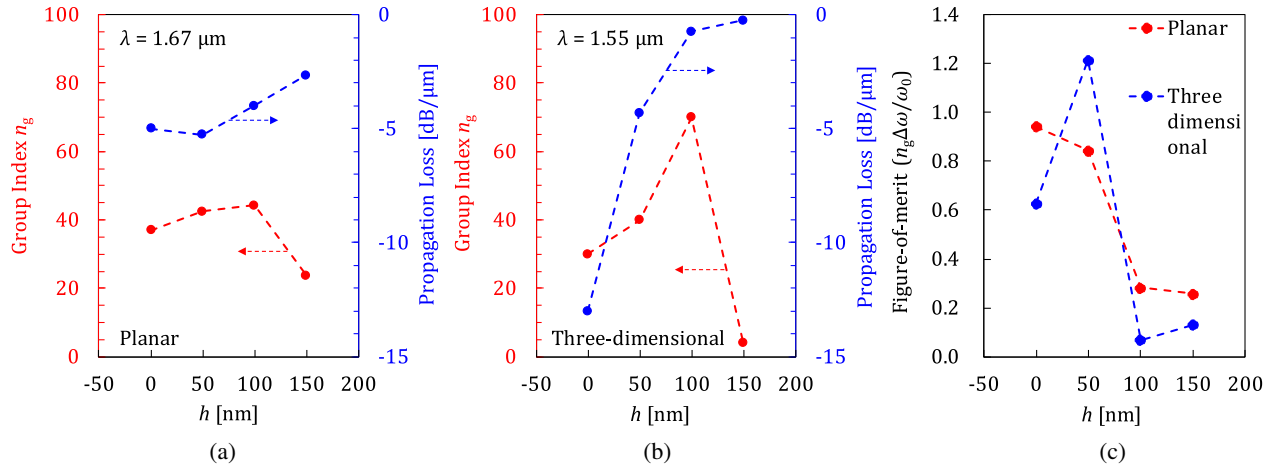

Fig. 8. Calculated group index and propagation loss per 1 μm as a function of the SiO_2 cladding layer thickness h for devices with a (a) planar metamaterial structure and (b) three-dimensional metamaterial structure; (c) derived FOM $n_g\Delta\omega/\omega_0$ as a function of h.

optical amplifiers (SOAs) [41] are one of the most promising solutions.

Another key figure of merit (FOM) for these slow-light devices is the delay bandwidth. Figure 8(c) shows the FOM $n_g\Delta\omega/\omega_0$ as a function of h, where $\Delta\omega$ and $\omega 0$ are the full width at half-maximum (FWHM) and the center angular frequency of the group index spectrum, respectively. Although the maximum value of the group index increases with the increase of the thickness of the cladding layer h, the delay bandwidth becomes narrower. Taking this trade-off into the consideration, the most FOM was obtained when $h = 0$ nm and 50 nm for the planar structure and the three-dimensional structure, respectively.

5. CONCLUSION

In this paper, two types of slow-light Si waveguides with metamaterials (planar and three-dimensional) were proposed, and the dispersion relation was analyzed by using the homogenization-based mode analysis method. The maximum group index and the propagation loss for each distance between the Si core and the homogenized region h were derived, and the highest group index of ∼70 was achieved near the resonant frequency (∼193 THz) with the propagation loss of ∼0.7 dB/μm by setting $h = 100$ nm for the device with a three-dimensional metamaterial structure. The results reveal that a delay time of ∼1 ps can be achieved within a 3-dB signal loss by using the metamaterial waveguide.

Funding. Japan Science and Technology Agency (JST); Core Research for Evolutional Science and Technology (CREST) (JPMJCR15N6); Japan Society for the Promotion of Science (JSPS) (15H05763, 15J11774, 16H06082, 16J11581, 17H03247).

REFERENCES

1. S. Linden, C. Enkrich, G. Dolling, M. W. Klein, J. Zhou, T. Koschny, C. M. Soukoulis, S. Burger, F. Schmidt, and M. Wegener, "Photonic metamaterials: magnetism at optical frequencies," IEEE J. Sel. Top. Quantum Electron. **12**, 1097–1105 (2006).
2. H. J. Lezec, J. A. Dionne, and H. A. Atwater, "Negative refraction at visible frequencies," Science **316**, 430–432 (2007).
3. J. B. Pendry, D. Schurig, and D. R. Smith, "Controlling electromagnetic fields," Science **312**, 1780–1782 (2006).
4. D. Schurig, J. J. Mock, B. J. Justice, S. A. Cummer, J. B. Pendry, A. F. Starr, and D. R. Smith, "Metamaterial electromagnetic cloak at microwave frequencies," Science **314**, 977–980 (2006).
5. L. H. Gabrielli, J. Cardenas, C. B. Poitras, and M. Lipson, "Silicon nanostructure cloak operating at optical frequencies," Nat. Photonics **3**, 461–463 (2009).
6. N. Landy and D. R. Smith, "A full-parameter unidirectional metamaterial cloak for microwaves," Nat. Mater. **12**, 25–28 (2013).
7. T. Amemiya, M. Taki, T. Kanazawa, T. Hiratani, and S. Arai, "Optical lattice model towards nonreciprocal invisibility cloaking," IEEE J. Quantum Electron. **51**, 1–10 (2015).
8. Z. Jacob, L. V. Alekseyev, and E. Narimanov, "Optical hyperlens: far-field imaging beyond the diffraction limit," Opt. Express **14**, 8247–8256 (2006).
9. W. T. Chen, K.-Y. Yang, C.-M. Wang, Y.-W. Huang, G. Sun, I.-D. Chiang, C. Y. Liao, W.-L. Hsu, H. T. Lin, S. Sun, L. Zhou, A. Q. Liu, and D. P. Tsai, "High-efficiency broadband meta-hologram with polarization-controlled dual images," Nano Lett. **14**, 225–230 (2014).
10. T. Amemiya, T. Kanazawa, S. Yamasaki, and S. Arai, "Metamaterial waveguide devices for integrated optics," Materials **10**, 1037 (2017).
11. K. L. Tsakmakidis, A. D. Boardman, and O. Hess, "'Trapped rainbow' storage of light in metamaterials," Nature **450**, 397–401 (2007).
12. H. Hu, D. Ji, X. Zeng, K. Liu, and Q. Gan, "Rainbow trapping in hyperbolic metamaterial waveguide," Sci. Rep. **3**, 1249 (2013).
13. T. Amemiya, A. Ishikawa, T. Kanazawa, J. Kang, N. Nishiyama, Y. Miyamoto, T. Tanaka, and S. Arai, "Permeability-controlled optical modulator with tri-gate metamaterial: control of permeability on InP-based photonic integration platform," Sci. Rep. **5**, 8985 (2015).
14. Z. J. Wong, Y.-L. Xu, J. Kim, K. O'Brien, Y. Wang, L. Feng, and X. Zhang, "Lasing and anti-lasing in a single cavity," Nat. Photonics **10**, 796–801 (2016).
15. Z. Li, M.-H. Kim, C. Wang, Z. Han, S. Shrestha, A. C. Overvig, M. Lu, A. Stein, A. M. Agarwal, M. Lončar, and N. Yu, "Controlling propagation and coupling of waveguide modes using phase-gradient metasurfaces," Nat. Nanotechnol. **12**, 675–683 (2017).
16. R. Guo, M. Decker, F. Setzpfandt, X. Gai, D.-Y. Choi, R. Kiselev, A. Chipouline, I. Staude, T. Pertsch, D. N. Neshev, and Y. S. Kivshar, "High-bit rate ultra-compact light routing with mode-selective on-chip nanoantennas," Sci. Adv. **3**, e1700007 (2017).
17. M. J. R. Heck, H.-W. Chen, A. W. Fang, B. R. Koch, D. Liang, H. Park, M. N. Sysak, and J. E. Bowers, "Hybrid silicon photonics for optical interconnects," IEEE J. Sel. Top. Quantum Electron. **17**, 333–346 (2011).
18. J. K. Doylend and A. P. Knights, "The evolution of silicon photonics as an enabling technology for optical interconnection," Laser Photon. Rev. **6**, 504–525 (2012).
19. S. E. Harris, "Electromagnetically induced transparency," Phys. Today **50**(7), 36–42 (1997).
20. L. V. Hau, S. E. Harris, Z. Dutton, and C. H. Behroozi, "Light speed reduction to 17 metres per second in an ultracold atomic gas," Nature **397**, 594–598 (1999).
21. M. D. Lukin and A. Imamoğlu, "Controlling photons using electromagnetically induced transparency," Nature **413**, 273–276 (2001).
22. J. J. Longdell, E. Fraval, M. J. Sellars, and N. B. Manson, "Stopped light with storage times greater than one second using electromagnetically induced transparency in a solid," Phys. Rev. Lett. **95**, 063601 (2005).
23. Y. A. Vlasov, M. O'Boyle, H. F. Hamann, and S. J. McNab, "Active control of slow light on a chip with photonic crystal waveguides," Nature **438**, 65–69 (2005).
24. T. Baba, "Slow light in photonic crystals," Nat. Photonics **2**, 465–473 (2008).
25. X. Xiao, H. Xu, X. Li, Z. Li, T. Chu, Y. Yu, and J. Yu, "High-speed, low-loss silicon Mach-Zehnder modulators with doping optimization," Opt. Express **21**, 4116–4125 (2013).
26. W. Bogaerts, P. Dumon, D. V. Thourhout, D. Taillaert, P. Jaenen, J. Wouters, S. Beckx, V. Wiaux, and R. G. Baets, "Compact wavelength-selective functions in silicon-on-insulator photonic wires," IEEE J. Sel. Top. Quantum Electron. **12**, 1394–1401 (2006).
27. J. Zhou, T. Koschny, M. Kafesaki, E. N. Economou, J. B. Pendry, and C. M. Soukoulis, "Saturation of the magnetic response of split-ring resonators at optical frequencies," Phys. Rev. Lett. **95**, 223902 (2005).
28. T. Amemiya, T. Shindo, D. Takahashi, S. Myoga, N. Nishiyama, and S. Arai, "Nonunity permeability in metamaterial-based GaInAsP/InP multimode interferometers," Opt. Lett. **36**, 2327–2329 (2011).
29. T. Amemiya, T. Shindo, D. Takahashi, N. Nishiyama, and S. Arai, "Magnetic interactions at optical frequencies in an InP-based waveguide device with metamaterial," IEEE J. Quantum Electron. **47**, 736–744 (2011).
30. T. Amemiya, S. Myoga, T. Shindo, E. Murai, N. Nishiyama, and S. Arai, "Permeability retrieval in InP-based waveguide optical device combined with metamaterial," Opt. Lett. **37**, 2301–2303 (2012).
31. D. R. Smith, D. C. Vier, T. Koschny, and C. M. Soukoulis, "Electromagnetic parameter retrieval from inhomogeneous metamaterials," Phys. Rev. E **71**, 036617 (2005).
32. D. R. Smith and J. B. Pendry, "Homogenization of metamaterials by field averaging (invited paper)," J. Opt. Soc. Am. B **23**, 391–403 (2006).

33. C. É. Kriegler, M. S. Rill, S. Linden, and M. Wegener, "Bianisotropic photonic metamaterials," IEEE J. Sel. Top. Quantum Electron. **16**, 367–375 (2010).
34. E. A. J. Marcatili, "Dielectric rectangular waveguide and directional coupler for integrated optics," Bell Syst. Tech. J. **48**, 2071–2102 (1969).
35. R. W. Pryor, *Multiphysics Modeling Using COMSOL: A First Principles Approach* (Jones & Bartlett, 2009).
36. T.-I. Jeon and D. Grischkowsky, "Nature of conduction in doped silicon," Phys. Rev. Lett. **78**, 1106–1109 (1997).
37. T. J. Cui and J. A. Kong, "Time-domain electromagnetic energy in a frequency-dispersive left-handed medium," Phys. Rev. B **70**, 205106 (2004).
38. P. Yao, C. V. Vlack, A. Reza, M. Patterson, M. M. Dignam, and S. Hughes, "Ultrahigh Purcell factors and Lamb shifts in slow-light metamaterial waveguides," Phys. Rev. B **80**, 195106 (2009).
39. Y. Terada, K. Miyasaka, H. Ito, and T. Baba, "Slow-light effect in a silicon photonic crystal waveguide as a sub-bandgap photodiode," Opt. Lett. **41**, 289–292 (2016).
40. O. Hess, J. B. Pendry, S. A. Maier, R. F. Oulton, J. M. Hamm, and K. L. Tsakmakidis, "Active nanoplasmonic metamaterials," Nat. Mater. **11**, 573–584 (2012).
41. E. S. Bjorlin, T. Kimura, Q. Chen, C. Wang, and J. E. Bowers, "High output power 1540 nm vertical cavity semiconductor optical amplifiers," Electron. Lett. **40**, 121–123 (2004).